PHOTONICS Research

Femtosecond mode-locking of a fiber laser using a $CoSb_3$-skutterudite-based saturable absorber

Jinho Lee, Yoontaek Kim, Kyungtaek Lee, and Ju Han Lee*

School of Electrical and Computer Engineering, University of Seoul, Seoul 02504, South Korea
*Corresponding author: j.h.lee@ieee.org

Received 1 June 2018; revised 16 July 2018; accepted 24 July 2018; posted 25 July 2018 (Doc. ID 334216); published 10 September 2018

We experimentally demonstrate an ultrafast mode-locker based on a $CoSb_3$ skutterudite topological insulator for femtosecond mode-locking of a fiber laser. The mode-locker was implemented on a side-polished fiber platform by depositing a $CoSb_3$/PVA composite. The measured modulation depth and saturation power for the transverse-electric mode input were ~5% and ~8.7 W, respectively, and ~2.8% and ~10.6 W for the transverse-magnetic mode input. By incorporating this mode-locker into an erbium-doped fiber-based ring cavity, we were able to readily generate mode-locked, soliton pulses having a pulse width of ~833 fs at 1557.9 nm. The 3-dB bandwidth of the output pulses and time-bandwidth product were ~3.44 and 0.353 nm, respectively. To the best of the authors' knowledge, this is the first demonstration of the use of a skutterudite-based saturable absorber for femtosecond mode-locked pulse generation.

OCIS codes: (140.3510) Lasers, fiber; (140.4050) Mode-locked lasers; (160.4330) Nonlinear optical materials.

https://doi.org/10.1364/PRJ.6.000C36

1. INTRODUCTION

Ultrafast pulsed lasers have served as a useful light source in many applications such as micromachining, spectroscopy, and laser surgery [1,2]. In particular, the usage of the optical-fiber-based laser technology has attracted considerable technical attention in recent years due to its range of advantages including the alignment-free operation, high beam quality, environmental stability, and compactness [3].

A commonly used method for the generation of ultrafast pulses from fiber-laser cavities is passive mode-locking. Passive mode-locking is usually realized within the fiberized cavities using either of the two nonlinear optical phenomena, nonlinear polarization rotation (NPR) or saturable absorption. Saturable absorption is a nonlinear optical phenomenon wherein the light absorption decreases with the increase of the light intensity. Saturable absorption allows for a more stable mode-locking operation compared with NPR under changing environmental conditions. Until now, saturable-absorption properties have been identified for a variety of optical materials; for example, III-V compound semiconductors [4], carbon nanotubes (CNTs) [5–9], graphene [10–15], graphene oxide (GO) [16–20], graphite [21–23], topological insulators (TIs) [21–32], transition metal dichalcogenides (TMDCs) [33–47], gold nanoparticles [48–53], black phosphorus (BP) [54–57], MXene [58], antimonene [59], and bismuthene [60]. In particular, the authors' group found that filled skutterudites (FSs) can also serve as an efficient saturable-absorption material and reported their potential as the base material for the implementation of a fast saturable absorber (SA) [61].

Skutterudites have been extensively investigated regarding their thermoelectric applications due to their low cost, high thermoelectric quality, wide operating-temperature range, long-term thermoelectric stability, and reasonably sound mechanical performance [62–64]. The general chemical formula of the common binary skutterudites is TX_3, where T is a group-9 transition metal such as cobalt (Co), rhodium (Rh), or iridium (Ir), and X is a pnicogen such as phosphorous (P), arsenic (As), or antimony (Sb). These compounds comprise a body-centered cubic structure composed of 32 unit-cell atoms, and its space group is Im3. Since the skutterudite thermal conductivity is too large, it typically needs to be reduced by filling the cage-like voids with an electropositive element, thereby forming a stabilized compound [65]; this compound is the filled skutterudite, the formula of which is $M_yT_4X_{12}$. The commonly used filling elements are the atoms of the rare-earth, alkali-earth, and group-14 carbon-family elements; indium (In), cadmium (Cd), and silver (Ag) atoms have also been used for this purpose.

Recently, the authors' group investigated the electric-band structures of the unfilled and filled skutterudites of cobalt antimonide ($CoSb_3$) and $In_{0.2}Co_4Sb_{12}$, respectively, using the density functional theory (DFT) calculation to calculate their ultimate potential regarding the base saturable-absorption

materials [66]. Notably, the $CoSb_3$ skutterudite with a small bandgap and a high carrier mobility [67] was identified as a TI [68–70]. TIs exhibit the gapless metallic states on the surface with the insulating interior, due to the combination of strong spin-orbit coupling-induced band inversion and time-reversal symmetry. Such unique properties enable these new Dirac materials to exhibit extraordinary charge and spin properties at their edges and surfaces [71]. It should be noted that the TIs generally possess sound thermoelectric properties, while it is already known that the key ingredients of the thermoelectric materials and the topological insulators are the same. Sound thermoelectric materials require a high electrical conductivity and a low thermal conductivity, both of which can be achieved by the narrow electronic bandgap and the large atomic masses. The band inversion substantially increases with the atomic mass, and the prerequisite condition for the band inversion is a narrow bandgap.

In this work, the ultimate potential of the $CoSb_3$ skutterudite as a fast mode-locker usable for femtosecond mode-locking is investigated as an ongoing study of the authors' group [59]. More specifically, the proposed mode-locker was implemented by the deposition of a composite film of the $CoSb_3$ skutterudite and polyvinyl alcohol (PVA) onto the flat side of the side-polished fiber. Its mode-locking performance was evaluated within the erbium-doped-fiber (EDF)-based ring cavity. To properly determine the material properties, a series of measurements including Raman spectroscopy, energy dispersive spectroscopy (EDS), scanning electron microscopy (SEM), X-ray photoelectron spectroscopy (XPS), wideband linear absorption, and nonlinear absorption were conducted. Consequently, stable mode-locked pulses with a temporal width of ~833 fs could readily be generated from the fiber laser at a wavelength of 1557.9 nm.

2. PREPARATION AND CHARACTERIZATION OF THE $CoSb_3$-BASED SATURABLE ABSORBER

$CoSb_3$ powder (99.9%; Toshima, Japan), which is a commercially available, low-cost powder, was used as the starting material. Raman spectroscopy, EDS, SEM, and XPS were conducted to determine the material properties of the prepared $CoSb_3$ particles. For these measurements, a small amount of a water-dispersed $CoSb_3$ particle was dropped and dried on top of the slide glass. First, the Raman spectrum was measured at 532 nm, and seven Raman peaks were observed, as shown in Fig. 1(a). Among them, the peaks at 83, 110, 136, 152, and 179 cm^{-1} were identified as the skutterudite phonon modes [72–74]. The peaks at ~186.7 cm^{-1} and ~255 cm^{-1} are the F_{2g} mode and the A_{1g} mode of Sb_2O_3, respectively [75,76]. Next, the EDS profile was measured, and the result is shown in Fig. 1(b). The spectrum shows strong peaks corresponding to cobalt (Co) and antimony (Sb), and the atomic ratio of the Co to the Sb is approximately 1:3 [77]. An SEM measurement for the detailed surface morphology of the $CoSb_3$ powder has been performed, as shown in the inset of Fig. 1(b). The size of the $CoSb_3$ particles is less than 75 μm. Then, the XPS particle measurement was performed. Figure 2(a) shows the high-resolution Co-2p spectrum, whereas the Sb-3d spectrum is shown in Fig. 2(b). The peak at ~778 eV in the

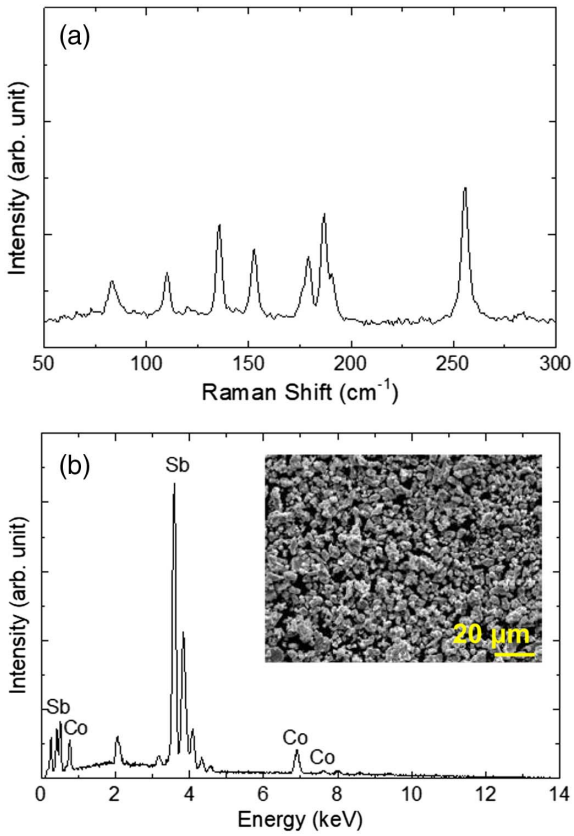

Fig. 1. Measured (a) Raman spectrum and (b) energy-dispersive X-ray spectroscopy (EDS) profile of the cobalt antimonide ($CoSb_3$) particle. Inset: measured SEM image of the prepared $CoSb_3$ powder.

Co-2p region of Fig. 2(a) is consistent with the reported binding-energy value of the Co $2p_{3/2}$ [60], while the peaks at 527.4 and 536.8 eV in the Sb-3d region of Fig. 2(b) are consistent with those of the Sb $3d_{5/2}$ and the Sb $3d_{3/2}$ [78,79]. It should be noted that the additional peaks at ~529.7 and ~539.1 eV in the Sb-3d region correspond to antimony trioxide (Sb_2O_3) [79,80]. The Raman and XPS measurements clearly show that the used $CoSb_3$ became substantially oxidized.

To implement an all-fiberized SA based on the prepared $CoSb_3$/PVA composite, the side-polished fiber platform was employed. The cross-sectional structure of the prepared $CoSb_3$/PVA-deposited side-polished fiber is shown in Fig. 3(a). For the preparation of the side-polished fiber, one side of the single-mode fiber, which was fixed onto the V-grooved slide glass, was polished. The distance between the flat side and the fiber core was measured at ~10 μm using the microscope. As reported in Refs. [43,58], the optimum distance range between the edge of the core and the polished surface of the side-polished fiber was empirically found to be from ~7 to ~11 μm for the evanescent field interaction in the wavelength band of 1.5 μm. The interaction length between the evanescent field and the $CoSb_3$ layer was ~2 mm. The measured insertion loss and polarization-dependent loss (PDL) of the prepared side-polished fiber are ~0.9 dB and ~0.07 dB, respectively. The $CoSb_3$/PVA solution was deposited on the flat side of the side-polished fiber using

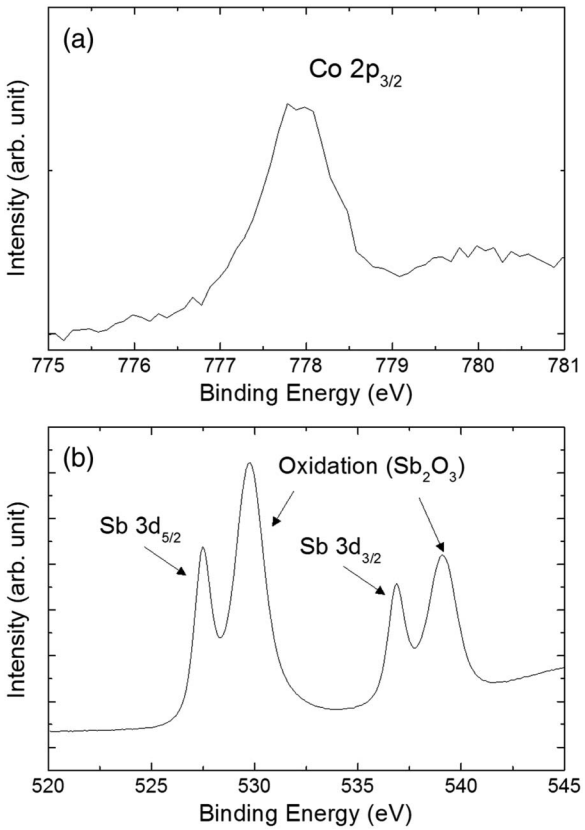

Fig. 2. Measured X-ray photoelectron spectroscopy (XPS) profiles: (a) cobalt (Co) 2p spectrum and (b) antimony (Sb) 3d spectrum of the $CoSb_3$ particle.

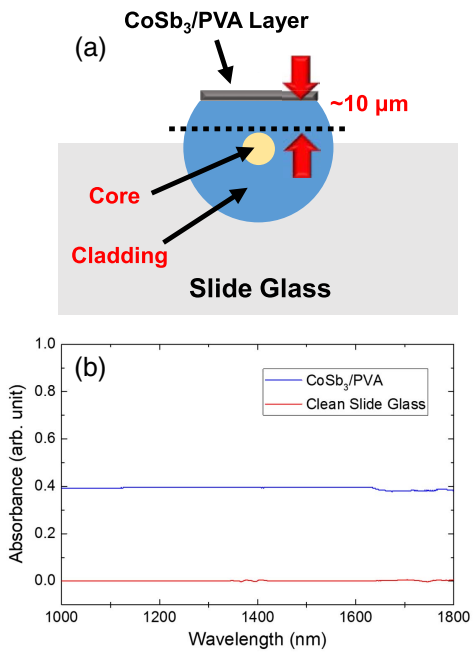

Fig. 3. (a) Schematic of the cobalt antimonide ($CoSb_3$)/polyvinyl alcohol (PVA)-deposited side-polished fiber. (b) Measured linear optical-absorption spectrum of the $CoSb_3$/PVA composite.

the solution-drop method and then dried at room temperature for 24 h.

Figure 3(b) shows the measured linear optical absorption of the $CoSb_3$/PVA composite film over the spectral range of 1000–1800 nm. For the linear absorption measurement for the $CoSb_3$/PVA composite, the $CoSb_3$/PVA solution was deposited onto a slide glass and then dried. After that, the linear absorption measurement was conducted using a spectrophotometer (UV-3600PLUS, Shimadzu). The linear absorbance of the slide glass without the $CoSb_3$/PVA composite was measured as a background reference. As shown in Fig. 3(b), a wide absorption range of light (1000–1800 nm) can be absorbed in the $CoSb_3$/PVA film, while the clean slide glass exhibits negligible absorption. Note that it is impossible to measure the linear transmittance of the clean side-polished fiber with the spectrophotometer used in our laboratory. After the composite deposition, the insertion loss and the PDL of the prepared side-polished fiber were increased up to ~3.4 dB and ~2.9 dB, respectively. We then launched a 1550 nm continuous wave (CW) amplified laser beam of 1 W power into our prepared $CoSb_3$-based SA to measure its damage threshold. We observed no damage of the prepared SA within the power level. Therefore, we believe that the damage threshold of the prepared $CoSb_3$-based SA must be larger than 1 W. However, it was impossible to measure the precise damage threshold value due to the limited availability of a high-power laser in our laboratory.

Next, the measurement of the nonlinear transmission curve as a function of the input-optical-pulse peak power was performed to determine the nonlinear absorption performance of the prepared $CoSb_3$/PVA-based SA. In order to measure the transmission curve of the prepared $CoSb_3$/PVA-based SA, we used our built mode-locked, 1.56-μm Er-doped fiber laser with a temporal width of ~730 fs at a repetition rate of ~22.26 MHz, and the measurement setup is shown in Fig. 4(a). The variable optical attenuator (VOA) was used to adjust the optical power of the mode-locked pulses. A 50:50 fiber-optic coupler was used to split the mode-locked pulses into two ports. One of the two ports was connected to the prepared $CoSb_3$/PVA-based SA, while the other was directly connected to a power meter to monitor the input optical power of the prepared SA. Another power meter was used to monitor the output power from the $CoSb_3$/PVA-based SA for its comparison with the input power. Since our SA had a non-negligible polarization-dependent loss of ~2.9 dB, a polarization controller (PC) was incorporated into the measurement setup. The nonlinear transmission curves were measured for the transverse-electric (TE) mode and the transverse-magnetic (TM) mode, respectively. Figures 4(b) and 4(c) show the transmission curves for the input-beams of the TE and TM modes, respectively, together with their corresponding fitting curves [81]

$$T(I) = 1 - \Delta T \cdot \exp\left(\frac{-I}{I_{\text{sat}}}\right) - T_{ns}, \tag{1}$$

where $T(I)$ is the transmission, ΔT is the modulation depth, I is the input-pulse energy, I_{sat} is the saturation energy, and T_{ns} is the nonsaturable loss. The estimated modulation depth and saturation power for the TE-mode input are ~5% and

~8.7 W, respectively, while they are ~2.8% and ~10.6 W for the TM-mode input. It is believed the modulation depth values of the fabricated $CoSb_3$/PVA-based SA are sufficiently high to induce mode-locking with the proper anomalous dispersion within the fiberized laser cavity [82]. It would be possible to increase the modulation depth by enlarging the interaction length and strength between the $CoSb_3$ particles and the oscillating beam. The interaction length increase could be easily obtained by polishing a longer length, and the interaction strength increase would need a further reduction of the distance between the core and the polished area. However, the two processes might increase the insertion loss of an SA. This means that there must exist an optimum structure of the side-polished fiber. And, in order to reduce the non-saturable loss, special care must be taken to reduce the surface roughness of the side-polished fiber, as well.

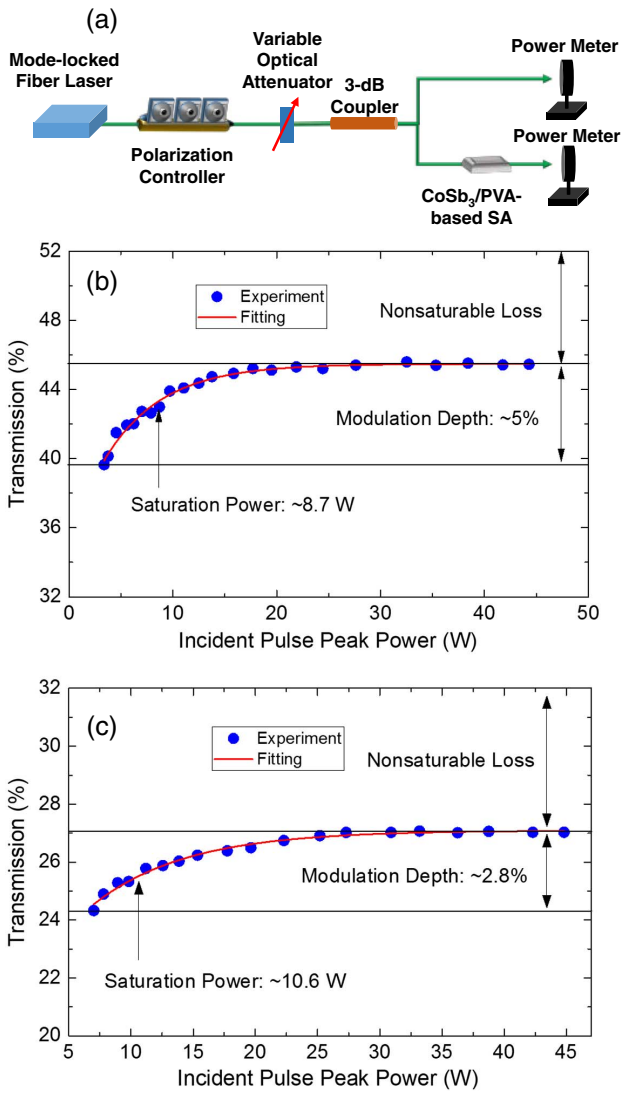

Fig. 4. (a) Measurement setup for nonlinear transmission curves of the $CoSb_3$/PVA-based SA. Measured nonlinear transmission curves of the $CoSb_3$/PVA-deposited side-polished fiber: (b) transverse electric (TE) mode and (c) transverse magnetic (TM) mode.

3. MODE-LOCKING OF A FIBER LASER WITH A $CoSb_3$/PVA-BASED SATURABLE ABSORBER

The experimental schematic of the proposed mode-locked EDF laser is shown in Fig. 5. The gain medium of the laser cavity is a 2.3-m-long EDF with a peak absorption of ~20 dB/m at a wavelength of 1530 nm. A 980-nm semiconductor laser diode was used as the pumping source, and the pump beam was launched into the gain fiber using a 980/1550-nm wavelength division multiplexer (WDM). The polarization-independent isolator was used to force the unidirectional light propagation. The mode-locked laser output was extracted from the ring cavity using the 10% port of the 90 : 10 coupler. A PC was used to optimize the polarization state within the laser cavity. The $CoSb_3$/PVA-deposited side-polished fiber was placed after the PC.

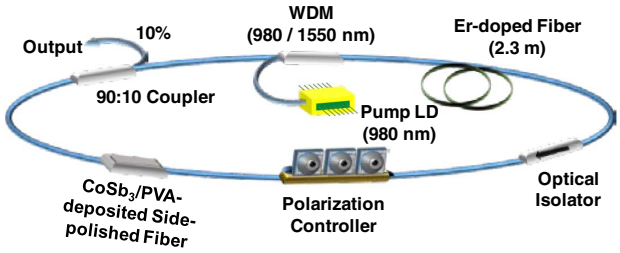

Fig. 5. Mode-locked fiber laser configuration.

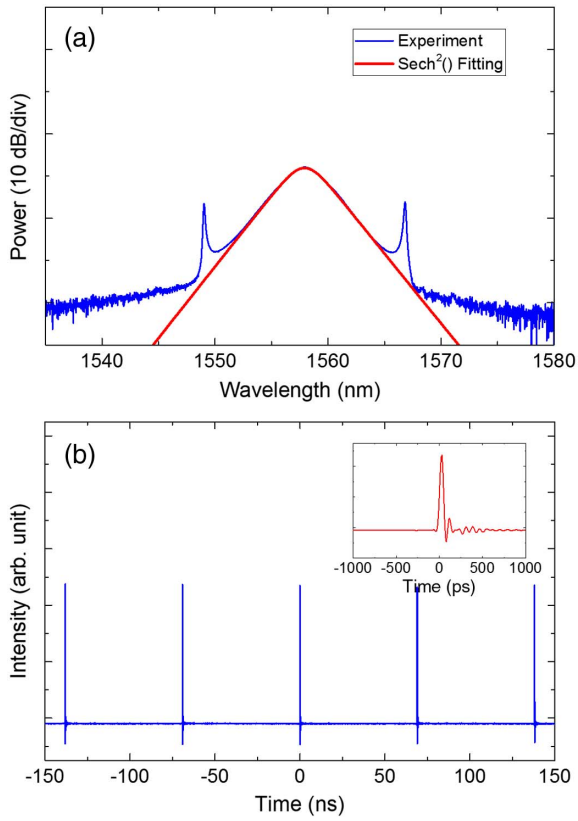

Fig. 6. Measured (a) optical spectrum (resolution bandwidth: 0.05 nm) and (b) oscilloscope trace of the output pulses. Inset: oscilloscope trace over the narrow span.

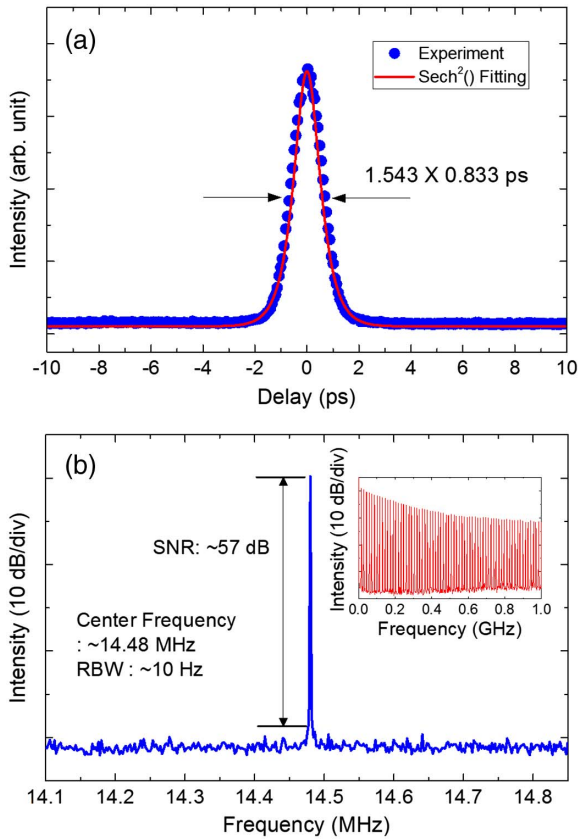

Fig. 7. Measured (a) autocorrelation trace of the output pulses and (b) electrical spectrum of the output pulses. Inset: measured electrical spectrum over a span of 1 GHz.

At a pump power of ~68 mW, the fundamental mode-locking started with multiple pulses (6 pulses), while the PC was carefully adjusted. When the pump power was reduced to ~21 mW, a single pulse stably appeared at the fundamental resonance frequency. The average output power was measured as ~0.1 mW. The main factors limiting the output power of this fiber laser are the insertion loss of the prepared $CoSb_3$-based SA and the coupling ratio of the output coupler. Furthermore, note that the insertion loss of the prepared SA is not a simple function of the material's property. In order to control the insertion loss of the prepared SA, we need to optimize the side-polished fiber platform in terms of interaction length, polishing depth, and concentration of the $CoSb_3$/PVA solution. Further investigations need to be conducted for the optimum performance of the laser.

Figure 6(a) shows the measured optical spectrum of the output mode-locked pulses. Kelly sidebands were clearly observed, indicating that the fiber laser operated in the soliton regime [83]. The center wavelength and the 3-dB bandwidth were measured as ~1557.9 nm and ~3.44 nm, respectively. Figure 6(b) shows the measured oscilloscope trace of the output pulses, while the inset of Fig. 6(b) shows the magnified view of the single output pulse. The pulse period is ~69.06 ns, corresponding to the fundamental repetition rate of ~14.48 MHz. For the oscilloscope measurements, a combination of the 16-GHz real-time oscilloscope and the 15-GHz photodetector was used.

Next, autocorrelation measurement was conducted using the two-photon absorption-based autocorrelator, and the measured autocorrelation trace is shown in Fig. 7(a) with the $sech^2()$ fitting curve. The estimated temporal width of the

Table 1. Performance Comparison Between the Present Work and the Previously Demonstrated Mode-Locked Erbium-Doped Fiber Lasers Incorporating Other Saturable Absorption Materials

Saturable Absorption Materials	SA Threshold Power	Modulation Depth (%)	Wavelength (nm)	3-dB Bandwidth (nm)	Repetition Rate (MHz)	Pulse Width (ps)	Output Power (mW)	Refs.
CNTs	NA	NA	1556.2	3.7	5.88	0.47	0.4	[6]
Graphene	NA	NA	1559	5.24	19.9	0.464	NA	[11]
Graphene	NA	NA	1561.6	1.96	6.99	1.3	NA	[12]
Graphene oxide	53 W[a]	5.25	1556.5	8.5	17.09	0.615	0.3	[20]
Bi_2Te_3	44 W[a]	15.7	1547	4.63	15.11	0.6	0.8	[28]
Bi_2Se_3	12 MW/cm^2[b]	3.9	1557.5	4.3	12.5	0.66	1.8	[31]
Sb_2Te_3	NA	NA	1558.6	1.8	4.75	1.8	0.5	[30]
MoS_2	137 MW/cm^2[b]	2.7	1556.3	6.1	463	0.935	5.9	[35]
WS_2	600 MW/cm^2[b]	0.95	1557	2.3	8.86	1.32	NA	[37]
$MoSe_2$	NA	1.4	1557.1	2.3	5.03	1.09	NA	[44]
WSe_2	NA	0.5	1557.6	2.1	5.31	1.25	NA	[44]
$MoTe_2$	NA	1.8	1561	2.4	5.26	1.2	NA	[46]
WTe_2	64.6 W[a]	2.85	1556.2	4.14	13.98	0.77	0.04	[47]
BP	6.55 MW/cm^2[b]	8.1	1571.45	2.9	5.96	0.946	NA	[54]
Gold nanorod	NA	4.9	1552	3.07	4.762	0.887	NA	[50]
Ti_3CN	45 W[a]	1.7	1557	5	15.4	0.66	0.05	[58]
Antimonene	10.8 mW[c]	6.4	1557.68	4.84	10.27	0.552	NA	[59]
Bismunene	30 MW/cm^2[b]	2.03	1559.18	4.64	8.83	0.652	1.15	[60]
$CoSb_3$	8.7 W[a]	5	1557.9	3.44	22.26	0.73	0.1	This work

NA: Not available.
[a]Saturation power.
[b]Saturation intensity.
[c]Average power.

output pulses is ~833 fs. Considering the 3-dB bandwidth of ~3.44 nm, the estimated time-bandwidth product is ~0.353, which is slightly higher than the 0.315 product of the transform-limited $sech^2()$ pulses, indicating that the output pulses are slightly chirped. The measured electrical spectrum of the output pulses is shown in Fig. 7(b). A sharp and strong peak with an electrical signal-to-background ratio of ~57 dB was observed at the fundamental frequency of 14.48 MHz in the electrical spectrum. The noise floor in Fig. 7(b) is −122 dBm. The inset of Fig. 7(b) shows the electrical spectrum with a 1-GHz frequency span. Strong beat signals were clearly observed, indicating that the output pulses are stable mode-locked pulses.

We believe that the dominant mechanism for mode-locking in our laser is saturable absorption, even if nonlinear rotation could partly contribute to the mode-locking. Note that Bogusławki *et al.* mentioned that a 2.7-dB PDL is small enough to exclude the NPR effect [84].

Lastly, we have summarized the performance of the $CoSb_3$-based SA in comparison with that of the SAs based on other saturable absorption materials, as shown in Table 1. Even if the $CoSb_3$-based SA does not outperform the SAs based on other saturable absorption materials in terms of SA threshold and modulation depth, it appears that it exhibits performance comparable to the others. The output average power of the mode-locked pulses from our laser was only 0.1 mW, which is smallest compared to those of the lasers incorporating the other saturable absorption materials.

4. CONCLUSION

It has been experimentally demonstrated in this study that the proposed $CoSb_3$/PVA-based SA can be used as a fast mode-locker for the generation of femtosecond-mode-locked pulses from the fiber laser. The SA was fabricated using a side-polished-fiber platform that was deposited with a $CoSb_3$/PVA composite. Stable mode-locked pulses with a temporal width of ~833 fs could be readily obtained from the EDF ring cavity. The authors believe that this experimental demonstration reveals the significant potential of the $CoSb_3$ TI in terms of ultrafast-laser technology.

Funding. National Research Foundation of Korea (NRF) (2018R1A2B6001641); Institute for Information and Communications Technology Promotion (IITP-2018-2015-0-00385).

REFERENCES

1. U. Keller, "Recent developments in compact ultrafast lasers," Nature **424**, 831–838 (2003).
2. K. Sugioka and Y. Cheng, "Ultrafast lasers—reliable tools for advanced materials processing," Light Sci. Appl. **3**, e149 (2014).
3. M. Fermann and I. Hartl, "Ultrafast fiber laser technology," IEEE J. Sel. Top. Quantum Electron. **15**, 191–206 (2009).
4. U. Keller, K. J. Weingarten, F. X. Kärtner, D. Kopf, B. Braun, I. D. Jung, R. Fluck, C. Hönninger, N. Matuschek, and J. A. der Au, "Semiconductor saturable absorber mirrors (SESAM's) for femtosecond to nanosecond pulse generation in solid-state lasers," IEEE J. Sel. Top. Quantum Electron. **2**, 435–453 (1996).
5. S. Y. Set, H. Yaguchi, Y. Tanaka, and M. Jablonski, "Laser mode locking using a saturable absorber incorporating carbon nanotubes," J. Lightwave Technol. **22**, 51–56 (2004).
6. Y.-W. Song, S. Yamashita, C. S. Goh, and S. Y. Set, "Carbon nanotube mode lockers with enhanced nonlinearity via evanescent field interaction in D-shaped fibers," Opt. Lett. **32**, 148–150 (2007).
7. M. Jung, J. Koo, Y. M. Chang, P. Debnath, Y.-W. Song, and J. H. Lee, "An all fiberized, 1.89-μm *Q*-switched laser employing carbon nanotube evanescent field interaction," Laser Phys. Lett. **9**, 669–673 (2012).
8. K. Kieu and F. W. Wise, "Soliton thulium-doped fiber laser with carbon nanotube saturable absorber," IEEE Photon. Technol. Lett. **21**, 128–130 (2009).
9. M. A. Chernysheva, A. A. Krylov, P. G. Kryukov, N. R. Arutyunyan, A. S. Pozharov, E. D. Obraztsova, and E. M. Dianov, "Thulium-doped mode-locked all-fiber laser based on NALM and carbon nanotube saturable absorber," Opt. Express **20**, B124–B130 (2012).
10. Q. Bao, H. Zhang, Y. Wang, Z. Ni, Y. Yang, Z. X. Shen, K. P. Loh, and D. Y. Tang, "Atomic-layer graphene as a saturable absorber for ultrafast pulsed lasers," Adv. Funct. Mater. **19**, 3077–3083 (2009).
11. Z. Sun, T. Hasan, F. Torrisi, D. Popa, G. Privitera, F. Wang, F. Bonaccorso, D. M. Basko, and A. C. Ferrari, "Graphene mode-locked ultrafast laser," ACS Nano **4**, 803–810 (2010).
12. Y.-W. Song, S.-Y. Jang, W.-S. Han, and M.-K. Bae, "Graphene mode-lockers for fiber lasers functioned with evanescent field interaction," Appl. Phys. Lett. **96**, 051122 (2010).
13. A. Martinez and Z. Sun, "Nanotube and graphene saturable absorber for fibre lasers," Nat. Photonics **7**, 842–845 (2013).
14. J. Ma, G. Q. Xie, P. Lv, W. L. Gao, P. Yuan, L. J. Qian, H. H. Yu, H. J. Zhang, J. Y. Wang, and D. Y. Tang, "Graphene mode-locked femtosecond laser at 2 μm wavelength," Opt. Lett. **37**, 2085–2087 (2012).
15. G. Sobon, J. Sotor, I. Pasternak, A. Krajewska, W. Strupinski, and K. M. Abramski, "Thulium-doped all-fiber laser mode-locked by CVD-graphene/PMMA saturable absorber," Opt. Express **21**, 12797–12802 (2013).
16. J. Xu, J. Liu, S. Wu, Q.-H. Yang, and P. Wang, "Graphene oxide mode-locked femtosecond erbium-doped fiber lasers," Opt. Express **20**, 15474–15480 (2012).
17. M. Jung, J. Koo, P. Debnath, Y.-W. Song, and J. H. Lee, "A mode-locked 1.91 μm fiber laser based on interaction between graphene oxide and evanescent field," Appl. Phys. Express **5**, 112702 (2012).
18. M. Jung, J. Koo, J. Park, Y.-W. Song, Y. M. Jhon, K. Lee, S. Lee, and J. H. Lee, "Mode-locked pulse generation from an all-fiberized, Tm-Ho-codoped fiber laser incorporating a graphene oxide-deposited side-polished fiber," Opt. Express **21**, 20062–20072 (2013).
19. J. Lee, J. Koo, P. Debnath, Y.-W. Song, and J. H. Lee, "A *Q*-switched, mode-locked fiber laser using a graphene oxide-based polarization sensitive saturable absorber," Laser Phys. Lett. **10**, 035103 (2013).
20. S. Ko, J. Lee, J. Koo, B. S. Joo, M. Gu, and J. H. Lee, "Chemical wet etching of an optical fiber using a hydrogen fluoride-free solution for a saturable absorber based on the evanescent field interaction," J. Lightwave Technol. **34**, 3776–3784 (2016).
21. G.-R. Lin and Y.-C. Lin, "Directly exfoliated and imprinted graphite nano-particle saturable absorber for passive mode-locking erbium-doped fiber laser," Laser Phys. Lett. **8**, 880–886 (2011).
22. Y.-H. Lin and G.-R. Lin, "Free-standing nano-scale graphite saturable absorber for passively mode-locked erbium doped fiber ring laser," Laser Phys. Lett. **9**, 398–404 (2012).
23. J. Lee, J. Lee, J. Koo, and J. H. Lee, "Graphite saturable absorber based on the pencil-sketching method for *Q*-switching of an erbium fiber laser," Appl. Opt. **55**, 303–309 (2016).
24. F. Bernard, H. Zhang, S. P. Gorza, and P. Emplit, "Towards mode-locked fiber laser using topological insulators," in *Nonlinear Photonics*, OSA Technical Digest (Optical Society of America, 2012), paper NTh1A.5.
25. C. Zhao, H. Zhang, X. Qi, Y. Chen, Z. Wang, S. Wen, and D. Tang, "Ultra-short pulse generation by a topological insulator based saturable absorber," Appl. Phys. Lett. **101**, 211106 (2012).
26. Y. Chen, C. Zhao, H. Huang, S. Chen, P. Tang, Z. Wang, S. Lu, H. Zhang, S. Wen, and D. Tang, "Self-assembled topological insulator: Bi_2Se_3 membrane as a passive *Q*-switcher in an erbium-doped fiber laser," J. Lightwave Technol. **31**, 2857–2863 (2013).

27. H. Yu, H. Zhang, Y. Wang, C. Zhao, B. Wang, S. Wen, H. Zhang, and J. Wang, "Topological insulator as an optical modulator for pulsed solid-state lasers," Laser Photon. Rev. **7**, L77–L83 (2013).
28. J. Lee, J. Koo, Y. M. Jhon, and J. H. Lee, "A femtosecond pulse erbium fiber laser incorporating a saturable absorber based on bulk-structured Bi_2Te_3 topological insulator," Opt. Express **22**, 6165–6173 (2014).
29. M. Jung, J. Lee, J. Koo, J. Park, Y.-W. Song, K. Lee, S. Lee, and J. H. Lee, "A femtosecond pulse fiber laser at 1935 nm using a bulk-structured Bi_2Te_3 topological insulator," Opt. Express **22**, 7865–7874 (2014).
30. J. Sotor, G. Sobon, W. Macherzynski, P. Paletko, K. Grodecki, and K. M. Abramski, "Mode-locking in Er-doped fiber laser based on mechanically exfoliated Sb_2Te_3 saturable absorber," Opt. Mater. Express **4**, 1–6 (2014).
31. H. Liu, X.-W. Zheng, M. Liu, N. Zhao, A.-P. Luo, Z.-C. W.-C. Xu, H. Zhang, C.-J. Zhao, and S.-C. Wen, "Femtosecond pulse generation from a topological insulator mode-locked fiber laser," Opt. Express **22**, 6868–6873 (2014).
32. J. Lee, J. Lee, J. Koo, H. Chung, and J. H. Lee, "Linearly polarized, *Q*-switched, erbium-doped fiber laser incorporating a bulk-structured bismuth telluride/polyvinyl alcohol saturable absorber," Opt. Eng. **55**, 076109 (2016).
33. H. Zhang, S. B. Lu, J. Zheng, J. Du, S. C. Wen, D. Y. Tang, and K. P. Loh, "Molybdenum disulfide (MoS_2) as a broadband saturable absorber for ultra-fast photonics," Opt. Express **22**, 7249–7260 (2014).
34. S. Wang, H. Yu, H. Zhang, A. Wang, M. Zhao, Y. Chen, L. Mei, and J. Wang, "Broadband few-layer MoS_2 saturable absorbers," Adv. Mater. **26**, 3538–3544 (2014).
35. K. Wu, X. Zhang, J. Wang, and J. Chen, "463-MHz fundamental mode-locked fiber laser based on few-layer MoS_2 saturable absorber," Opt. Lett. **40**, 1374–1377 (2015).
36. R. I. Woodward, E. J. R. Kelleher, R. C. T. Howe, G. Hu, F. Torrisi, T. Hasan, S. V. Popov, and J. R. Taylor, "Tunable *Q*-switched fiber laser based on saturable edge-state absorption in few-layer molybdenum disulfide (MoS_2)," Opt. Express **22**, 31113–31122 (2014).
37. D. Mao, Y. Wang, C. Ma, L. Han, B. Jiang, X. Gan, S. Hua, W. Zhang, T. Mei, and J. Zhao, "WS_2 mode-locked ultrafast fiber laser," Sci. Rep. **5**, 7965 (2015).
38. M. Jung, J. Lee, J. Park, J. Koo, Y. M. Jhon, and J. H. Lee, "Mode-locked, 1.94-μm, all-fiberized laser using WS_2 based evanescent field interaction," Opt. Express **23**, 19996–20006 (2015).
39. P. Yan, A. Liu, Y. Chen, H. Chen, S. Ruan, C. Guo, S. Chen, I. L. Li, H. Yang, J. Hu, and G. Cao, "Microfiber-based WS_2-film saturable absorber for ultra-fast photonics," Opt. Mater. Express **5**, 479–489 (2015).
40. J. Lee, J. Park, J. Koo, Y. M. Jhon, and J. H. Lee, "Harmonically mode-locked femtosecond fiber laser using non-uniform, WS_2-particle deposited side-polished fiber," J. Opt. **18**, 035502 (2016).
41. B. Chen, X. Zhang, K. Wu, H. Wang, J. Wang, and J. Chen, "*Q*-switched fiber laser based on transition metal dichalcogenides MoS_2, $MoSe_2$, WS_2, and WSe_2," Opt. Express **23**, 26723–26737 (2015).
42. R. I. Woodward, R. C. T. Howe, T. H. Runcorn, G. Hu, F. Torrisi, E. J. R. Kelleher, and T. Hasan, "Wideband saturable absorption in few-layer molybdenum diselenide ($MoSe_2$) for *Q*-switching Yb-, Er- and Tm-doped fiber," Opt. Express **23**, 20051–20061 (2015).
43. J. Koo, J. Park, J. Lee, Y. M. Jhon, and J. H. Lee, "Femtosecond harmonic mode-locking of a fiber laser at 3.27 GHz using a bulk-like, $MoSe_2$-based saturable absorber," Opt. Express **24**, 10575–10589 (2016).
44. D. Mao, X. She, B. Du, D. Yang, W. Zhang, K. Song, X. Cui, B. Jiang, T. Peng, and J. Zhao, "Erbium-doped fiber laser passively mode locked with few-layer $WSe_2/MoSe_2$ nanosheets," Sci. Rep. **6**, 23583 (2016).
45. J. Lee, J. Koo, J. Lee, Y. M. Jhon, and J. H. Lee, "All-fiberized, femtosecond laser at 1912 nm using a bulk-like $MoSe_2$ saturable absorber," Opt. Mater. Express **7**, 2968–2979 (2017).
46. D. Mao, B. Du, D. Yang, S. Zhang, Y. Wang, W. Zhang, X. She, H. Cheng, H. Zeng, and J. Zhao, "Nonlinear saturable absorption of liquid-exfoliated molybdenum/tungsten ditelluride nanosheets," Small **12**, 1489–1497 (2016).
47. J. Koo, Y. I. Jhon, J. Park, J. Lee, Y. M. Jhon, and J. H. Lee, "Near-infrared saturable absorption of defective bulk-structured WTe_2 for femtosecond laser mode-locking," Adv. Funct. Mater. **26**, 7454–7461 (2016).
48. T. Jiang, Y. Xu, Q. Tian, L. Liu, Z. Kang, R. Yang, G. Qin, and W. Qin, "Passively *Q*-switching induced by gold nanocrystals," Appl. Phys. Lett. **101**, 151122 (2012).
49. Z. Kang, Q. Li, X. J. Gao, L. Zhang, Z. X. Jia, Y. Feng, G. S. Qin, and W. P. Qin, "Gold nanorod saturable absorber for passive mode-locking at 1 μm wavelength," Laser Phys. Lett. **11**, 035102 (2014).
50. X.-D. Wang, Z.-C. Luo, H. Liu, M. Liu, A.-P. Luo, and W.-C. Xu, "Microfiber-based gold nanorods as saturable absorber for femtosecond pulse generation in a fiber laser," Appl. Phys. Lett. **105**, 161107 (2014).
51. J. Koo, J. Lee, W. Shin, and J. H. Lee, "Large energy, all-fiberized *Q*-switched pulse laser using a GNRs/PVA saturable absorber," Opt. Mater. Express **5**, 1859–1867 (2015).
52. Z. Kang, M. Y. Liu, X. J. Gao, N. Li, S. Y. Yin, G. S. Qin, and W. P. Qin, "Mode-locked thulium-doped fiber laser at 1982 nm by using a gold nanorods saturable absorber," Laser Phys. Lett. **12**, 045105 (2015).
53. J. Lee, J. Koo, J. Lee, and J. H. Lee, "End-to-end self-assembly of gold nanorods in water solution for absorption enhancement at a 1-to-2 μm band for a broadband saturable absorber," J. Lightwave Technol. **34**, 5250–5257 (2016).
54. Y. Chen, G. Jiang, S. Chen, Z. Guo, X. Yu, C. Zhao, H. Zhang, Q. Bao, S. Wen, D. Tang, and D. Fan, "Mechanically exfoliated black phosphorus as a new saturable absorber for both *Q*-switching and mode-locking laser operation," Opt. Express **23**, 12823–12833 (2015).
55. Z.-C. Luo, M. Liu, Z.-N. Guo, X.-F. Jiang, A.-P. Luo, C.-J. Zhao, X.-F. Yu, W.-C. Xu, and H. Zhang, "Microfiber-based few-layer black phosphorus saturable absorber for ultra-fast fiber laser," Opt. Express **23**, 20030–20039 (2015).
56. K. Park, J. Lee, Y. T. Lee, W.-K. Choi, J. H. Lee, and Y.-W. Song, "Black phosphorus saturable absorber for ultrafast mode-locked pulse laser via evanescent field interaction," Ann. Phys. **527**, 770–776 (2015).
57. J. Sotor, G. Sobon, M. Kowalczyk, W. Macherzynski, P. Paletko, and K. M. Abramski, "Ultrafast thulium-doped fiber laser mode locked with black phosphorus," Opt. Lett. **40**, 3885–3888 (2015).
58. Y. I. Jhon, J. Koo, B. Anasori, M. Seo, J. H. Lee, Y. Gogotsi, and Y. M. Jhon, "Metallic MXene saturable absorber for femtosecond mode-locked lasers," Adv. Mater. **29**, 1702496 (2017).
59. Y. Song, Z. Liang, X. Jiang, Y. Chen, Z. Li, L. Lu, Y. Ge, K. Wang, J. Zheng, and S. Lu, "Few-layer antimonene decorated microfiber: ultra-short pulse generation and all-optical thresholding with enhanced long term stability," 2D Mater. **4**, 045010 (2017).
60. L. Lu, Z. Liang, L. Wu, Y. Chen, Y. Song, S. C. Dhanabalan, J. S. Pronraj, B. Dong, Y. Xiang, F. Xing, D. Fan, and H. Zhang, "Few-layer bismuthene: sonochemical exfoliation, nonlinear optics and applications for ultrafast photonics with enhanced stability," Laser Photon. Rev. **12**, 1870012 (2017).
61. J. Lee, B.-K. Yu, Y. I. Jhon, J. Koo, S. J. Kim, Y. M. Jhon, and J. H. Lee, "Filled skutterudites for broadband saturable absorbers," Adv. Opt. Mater. **5**, 1700096 (2017).
62. D. T. Morelli, T. Caillat, J.-P. Fleurial, A. Borshchevsky, J. Vandersande, B. Chen, and C. Uher, "Low-temperature transport properties of p-type $CoSb_3$," Phys. Rev. B **51**, 9622–9628 (1995).
63. J. Yang, M. G. Endres, and G. P. Meisner, "Valence of Cr in skutterudites: electrical transport and magnetic properties of Cr-doped $CoSb_3$," Phys. Rev. B **66**, 014436 (2002).
64. G. Rogl and P. Rogl, "Skutterudite, a most promising group of thermoelectric materials," Curr. Opin. Green Sustain. Chem. **4**, 50–57 (2017).
65. V. Keppens, D. Mandrus, B. C. Sales, B. C. Chakoumakos, P. Dai, R. Coldea, M. B. Maple, D. A. Gajewski, E. J. Freeman, and S. Bennington, "Localized vibrational modes in metallic solids," Nature **395**, 876–878 (1998).

66. Y. I. Jhon, J. Lee, Y. M. Jhon, and J. H. Lee, "Topological insulators for mode-locking of 2-μm fiber lasers," IEEE J. Sel. Top. Quantum Electron. **24**, 1102208 (2018).
67. T. Caillat, A. Borshchevsky, and J.-P. Fleurial, "Properties of single crystalline semiconducting $CoSb_3$," J. Appl. Phys. **80**, 4442–4449 (1996).
68. V. Pardo, J. C. Smith, and W. E. Pickett, "Linear bands, zero-momentum Weyl semimetal, and topological transition in skutterudite-structure pnictides," Phys. Rev. B **85**, 214531 (2012).
69. B. Yan, L. Müchler, X.-L. Qi, S.-C. Zhang, and C. Felser, "Topological insulators in filled skutterudites," Phys. Rev. B **85**, 165125 (2012).
70. M. Yang and W.-M. Liu, "The d-p band-inversion topological insulator in bismuth-based skutterudites," Sci. Rep. **4**, 5131 (2014).
71. M. Z. Hasan and C. L. Kane, "Colloquium: topological insulators," Rev. Mod. Phys. **82**, 3045–3067 (2010).
72. J. L. Feldman and D. J. Singh, "Lattice dynamics of skutterudites: first-principles and model calculations for $CoSb_3$," Phys. Rev. B **53**, 6273–6282 (1996).
73. X. Su, H. Li, G. Wang, H. Chi, X. Zhou, X. Tang, Q. Zhang, and C. Uher, "Structure and transport properties of double-doped $CoSb_{2.75}Ge_{0.25-x}Te_x$ (x = 0.125–0.20) with in situ nanostructure," Chem. Mater. **23**, 2948–2955 (2011).
74. L. X. Liu, H. Liu, J. Y. Wang, X. B. Hu, S. R. Zhao, H. D. Jiang, Q. J. Huang, H. H. Wang, and Z. F. Li, "Raman spectroscopy investigation of partially filled skutterudite," Chem. Phys. Lett. **347**, 373–377 (2001).
75. M. Bala, C. Pannu, S. Gupta, T. S. Tripathi, S. K. Tripathi, K. Asokan, and D. K. Aasthi, "Phase evolution and electrical properties of Co-Sb alloys fabricated from Co/Sb bilayers by thermal annealing and ion beam mixing," Phys. Chem. Chem. Phys. **17**, 24427–24437 (2015).
76. D. W. Zeng, C. S. Xie, B. L. Zhu, and W. L. Song, "Characteristics of Sb_2O_3 nanoparticles synthesized from antimony by vapor condensation method," Mater. Lett. **58**, 312–315 (2004).
77. O. L. Arnache, J. Pino, and L. C. Sánchez, "Determination of milling parameters useful on the formation of $CoSb_3$ thermoelectric powders by low-energy mechanical alloying," J. Mater. Sci. Mater. Electron. **27**, 4120–4130 (2016).
78. R. I. Hegde, S. R. Sainkar, S. Badrinarayanan, and A. P. B. Sinha, "A study of dilute tin alloys by X-ray photoelectron spectroscopy," J. Electron Spectrosc. Relat. Phenom. **24**, 19–25 (1981).
79. M. Bala, S. Gupta, S. K. Srivastava, S. Amrithapandian, T. S. Tripathi, S. K. Tripathi, C.-L. Dong, C.-L. Chen, D. K. Avasthi, and K. Asokan, "Evolution of nanostructured single-phase $CoSb_3$ thin films by low-energy ion beam induced mixing and their thermoelectric-performance," Phys. Chem. Chem. Phys. **19**, 24886–24895 (2017).
80. W. E. Morgan, W. J. Stec, and J. R. V. Wazer, "Inner-orbital binding-energy shifts of antimony and bismuth compounds," Inorg. Chem. **12**, 953–955 (1973).
81. K. Wu, B. Chen, X. Zhang, S. Zhang, C. Guo, C. Li, P. Xiao, J. Wang, L. Zhou, W. Zou, and J. Chen, "High-performance mode-locked and Q-switched fiber lasers based on novel 2D materials of topological insulators, transition metal dichalcogenides and black phosphorus: review and perspective," Opt. Commun. **406**, 214–229 (2018).
82. J. Jeon, J. Lee, and J. H. Lee, "Numerical study on the minimum modulation depth of a saturable absorber for stable fiber laser mode locking," J. Opt. Soc. Am. B **32**, 31–37 (2015).
83. S. M. J. Kelly, "Characteristic sideband instability of periodically amplified average soliton," Electron. Lett. **28**, 806–807 (1992).
84. J. Bogusławski, G. Soboń, R. Zybała, K. Mars, A. Mikuła, K. M. Abramski, and J. Sotor, "Investigation on pulse shaping in fiber laser hybrid mode-locked by Sb_2Te_3 saturable absorber," Opt. Express **23**, 29014–29023 (2015).